PHYSICS AND CHEMISTRY OF SOLID STATE
V. 26, No. 2 (2025) pp. 240-250
Section: Technology

DOI: 10.15330/pcss.26.2.240-250

Vasyl Stefanyk Precarpathian National University

ФІЗИКА І ХІМІЯ ТВЕРДОГО ТІЛА
Т. 26, № 2 (2025) С. 240-250
Технічні науки

PACS: 42.70.Qs

ISSN 1729-4428 (Print)
ISSN 2309-8589 (Online)

S. Fakhri-Mirzanagh[1], S.H. R. Shojaei[1,2], G. R. Pirgholi-Givi[3], Y. Azizian-Kalandaragh[4,5,6]

Theoretical and experimental study on the band gap of binary ZnS-CdS nanocomposites and expected best photocatalysts

[1]Department of Physics, Faculty of Science, Sahand University of Technology, Tabriz, Iran;
[2]X-LAB, Hasselt University, Agoralaan, Diepenbeek, Belgium, shojaei@sut.ac.ir;
[3]Department of Advanced Technologies, University of Mohaghegh Ardabili, Namin, Iran;
[4]Photonics Application and Research Center, Gazi University, Ankara, Turkey;
[5]Photonics Department, Applied Science Faculty, Gazi University, Ankara, Turkey;
[6]Department of Physics, University of Mohaghegh Ardabili, P.O. Box.179, Ardabil, Iran

In this study, ZnS-CdS nanocomposites were synthesized using a hydrothermal method to investigate their photocatalytic activity. The X-ray diffraction (XRD) results confirmed the formation of hexagonal structure for cadmium sulfide and zinc sulfide nanocomposites and the results of the scanning electron spectroscopy (SEM) indicated that by adding ZnS to cadmium sulfide's structure the size of the nanoparticles decreases, which is a clear sign of improved photocatalytic activity. Using absorption coefficient and UV-visible spectroscopy (UV), the band gap of pure CdS was obtained as 2.7 eV, by adding the Zn content the gap will decrease. The photocatalytic activity of prepared nanocomposites was studied by photodegradation of Rhodamine B (RhB) organic dye, and the synthesized sample with 0.1 M of zinc solution shows a smaller gap and size. In the next step, cadmium sulfide nanoparticles with different percentages of zinc were simulated and their HOMO-LUMO gaps were calculated by Density Functional Theory (DFT). In comparison to the other well-known functionals, it was found that M05 shows a better agreement with experimental results. The computational results confirm that the sample with 10% zinc content is a good candidate for photocatalytic activity.

Keywords: Hydrothermal, Photocatalytic, Rhodamine B, Gap, Density Functional Theory.

Received 26 July 2024; Accepted 10 April 2025.

Introduction

It is known that the ground state of systems can be determined using the density functional theory known as DFT. Born-Oppenheimer approximation presents that the most of molecular properties can be determined by exploring the electronic structure of the ground state and nuclear repulsion of a molecule. Ground state geometry, potential energy level, thermochemistry, and other physical and chemical properties are listed among these properties. Kohn-Sham's density functional theory has attracted more attention due to its features and advantages over the correlated wave function theory (WFT) [1-3]. Due to its rational computational costs, it was widely used in different scientific fields. It is known that the accuracy of DFT calculations is dependent on the exchange-correlation (XC) function [4]. Although the density functional theory works very well for some properties of molecules such as strong interactions between atoms and molecules, but in predicting some other properties such as weak interactions, dispersion, and Van Der Waals interactions, the DFT is not precise enough. In order to do a detailed study of the energy, geometry, and thermal properties of non-covalent interaction systems, numerous studies have been performed to produce a better functional [5-7]. For example, the well-known B3LYP (Becke, 3-parameter, Lee–Yang–Parr) functional: 1- It has better results for main group metals compared to transition metals. 2- It systematically underestimates reaction barrier

heights. 3- It is inaccurate for interactions dominated by medium-range correlation energy, such as van der Waals attraction, aromatic-aromatic stacking, and alkane isomerization energies. Therefore, new functionals such as M05 and M06 are used. M06-class functionals depend on spin-up and spin-down electron densities (i.e., spin densities), spin density gradients, spin kinetic energy densities, and, for nonlocal (also called hybrid) functionals, Hartree-Fock exchange. These functionals have 4 subsets*:* (a) M06, a hybrid meta functional, is a functional with good accuracy for transition metals, main group thermochemistry, and barrier heights; (b) M06-2X, another hybrid meta functional, is not good for transition metals but has excellent performance for main group chemistry, predicts accurate valence and Rydberg electronic excitation energies, and is an excellent functional for aromatic-aromatic stacking interactions; (c) M06-L is not as accurate as M06 for barrier heights but is the most accurate functional for transition metals (d) M06-HF is One of the good functionals for accurate calculation of the excited states of capacity, Rydberg, and charge transfer with a minimum reduction of ground state accuracy [8].

The bandgap is an important parameter in many optical and photovoltaic applications of different semiconducting systems. Based on the band gap, solids are divided into three categories: Insulator (with an extremely large band gap), conductor (almost zero band gap), and semiconductor (medium band gap energy) [9-11]. It is defined as the energy difference between the lowest energy of the conduction band and the highest energy of the valance band. This energy is also expressed as the minimum energy required to separate one electron from an N-electron system [12].

In theory, the value of electron affinity and ionization potential was found from the difference between the ground state energy of the N+1- electron system and the N-1-electron system with N-electron system, but in practice, it is obtained from the difference in the energy of orbitals HOMO (Highest Occupied Molecular Orbital) and LUMO (Lowest Unoccupied Molecular Orbital) [13-16]. In the LDA and GGA forms of DFT, the HOMO-LUMO gap equals the difference in the first derivatives of total energy with respect to the number of electrons, assuming that the total energy is a straight line between the states with unity and zero occupation [17]. In recent years, extensive research has been conducted using DFT functionals in periodic and non-periodic embedded cluster calculations to determine the band structure and other fundamental properties of systems [9, 18, 19]. Also, many other functionals such as many-body Green's function approximation (GW), the Bethe–Salpeter equation, as well as time-dependent density functional theory (TD-DFT), the calculated band gap is very precise. [20-22]. Also, researchers showed that the results obtained from Kohn-Sham's calculations for the band structure are different from the exact band gap [22]. B3LYP, PBE0, HSE, etc. functional calculations lead to improving the band gap value. It is shown that the historically first hybrid density functional, B3PW91, leads to dramatically better band gaps for the binary and ternary semiconductor compounds that are of interest in photovoltaics and thermo-electrics [23]. Recently, by combining experimental and theoretical methods, the band gap of the new class of materials were studied. In research by Hong et. al. $Pr_{4-x}Ca_xSi_{12}O_{3+x}N_{18-x}$ was prepared in monoclinic phase, and using the DFT method the band gap has been reported about 3.6 eV that has good agreement with experimental value (4.1 eV)[24]. In 2022, another study was carried out, and the results determined that the GGA and LDA methods do not provide correct values for the gap, but a functional HSE06 gives rise to an exact electronic structure characteristics for semiconductors [25].

A notable optical application of nanoparticles is their photocatalytic performance in water purification. The gap of a semiconducting photocatalyst is a critical parameter in evaluating its degradation efficiency. Any decrement in the gap size typically will increase the photocatalytic performance [26]. Oxide and sulfide nanomaterials are widely used in this field [27, 28], and among them, ZnS [29], CdS[30] and the their composites are mostly used as photocatalytic materials. The large band gap of ZnS (3.72–3.77 eV) restricts its activity to the UV region. However, it has demonstrated an excellent performance in hydrogen generation due to its high photon-to-electron conversion efficiency and significantly negative conduction band potential, which is well above the proton reduction potential [31]. To enhance the activity of these nanoparticles in the visible region, they were combined with different percentages of metal oxides or sulfides [32, 33]. Recent researches showed that by mixing the ZnS and CdS [34], the photocatalytic activity of the composite will certainly improve, and the degradation percentage depends on the relative proportion of the two ingredients. [33, 35, 36]. Considering the importance of the Zn percentage in the prepared nanocomposites for their photocatalytic activity, these nanocomposites must ultimately be synthesized with various Zn concentrations and this is a costly and time consuming process. While by simulating nanocomposites with different molecular ratios, the optimal material can be identified. In these studies, the band gap and band edges of ZnS-CdS nanocomposites with varying ratios were calculated using DFT functionals such as M05, M06, B3LYP, M06-L, and M06-2X, and the results were compared with experimental data.

Considering the fundamental similarities and differences between the HOMO-LUMO gap and the band gap, which arise from discrete molecular orbitals and Bloch states in extended periodic systems, respectively, and taking into account the size of our nanostructures, we conducted a comparative analysis between the experimentally measured band gap and the theoretically calculated HOMO-LUMO gap.

I. Method

1.1. Experimental

In this work, CdS nanoparticles and ZnS-CdS nanoparticles were prepared using a low-cost hydrothermal method. 0.1M of Cadmium acetate dihydrate (Merck) and 0.1M zinc acetate dihydrate (Merck) dispersed in 40 ml deionized water and mixed together for 20 min under a magnetic stirrer. Then, the

Table 1.

Miler index and related angle in XRD analysis

Semiconductor	2Θ°	Miler index	Semiconductor	2Θ°	Miler index
CdS	24.90	(1 0 0)	ZnS	24.90	(0 1 0)
	26.90	(0 0 2)		26.90	(0 0 2)
	28.1	(1 0 1)		28.1	(1 0 1)
	36.50	(1 1 0)		48.06	(1 1 0)
	46.72	(1 0 3)		51.78	(1 0 3)
	48.06	(2 0 0)			
	51.78	(1 1 2)			

prepared suspension was subjected to ultrasound waves for 30 minutes, after this step, 0.1M of Na_2S was added to the suspension drop by drop in 30 min, at the end, the prepared solution was placed in an autoclave in 180°C for 24 hours. The synthesized nanopowders washed 5 time by the water and dried under a temperature of 50°C in the oven. For preparation, the pure CdS and ZnS-CdS 0.05M, without zinc acetate dihydrate and by 0.05M of zinc acetate dihydrate all steps were repeated exactly with the same procedure.

1.2. Photocatalytic activity

In this research, Rhodamine B(RhB) has been used as a pollutant to investigate the photocatalytic activity of the prepared nanomaterials. 0.1g of the prepared nanopowder was spilled in the 100ml of 10ppm solution of Rhodamine B (RhB). The prepared solution was kept in absolute darkness for 30 minutes to reach equilibrium, then it was placed under direct SMD lamp 250W irradiation by λ>420nm. The temperature was fixed at 25 degrees Celsius by a water circulation device. Then after 15 minutes of light irradiation, 4 ml of the original solution was separated, and its nano-materials were deposited by centrifuge and its UV-visible spectrum was recorded. The main peak of RhB at 553 nm was checked after 15 minutes and then remained added to the original solution, which was done until the complete degradation of the pollutant.

1.3. Methodology

In our study, the spherical structure is designed in the hexagonal phase of cadmium sulfide and ZnS-CdS semiconductors with different Zn content, namely, 2.5%, 5%,10%, 15%, 20%, and 22.5% of Zn.

All calculations were performed using Gaussian16 software. Each of these 7 structures was optimized at the same level of theory. Default settings were considered in all calculations. In order to find the best functional, Multiple functional including B3LYP, M05, M06, M06-L and M06-2X, were employed in DFT calculations using unique basis set, LANL2DZ. For converging the geometry of the prepared structure, the SCF = (QC, novaracc, noincfock) command has been used.

1.4. Characterization

All samples were prepared using an ultrasound device (JAPAN NASIR-IRAN). X-ray diffraction (XRD) analysis was performed with a Philips X'Pert instrument utilizing Cu Kα radiation (λ = 1.5406 Å). The absorbance spectra were examined using a UV-1800 Shimadzu spectrophotometer. The morphology and size effects were analyzed with a MIRA3 FEG-SEM device.

II. Results and Discussion

2.1. XRD characterization

X-ray diffraction characterization is carried out to check the phases and crystallinity of prepared nanoparticles, so in Figure 1, the XRD pattern of prepared samples has been shown. The pattern is matched by 96-901-1664 reference code. In this process, CdS nanoparticles were crystalized in hexagonal phases by P63mc space group. Peaks of ZnS nanoparticles have overlapped with CdS peaks and made the peaks sharper Also, it has caused the displacement of some peaks, the ZnS nanoparticles were synthetized in hexagonal phase [37] within CdS structure. Miler indexes of CdS and ZnS are presented in table 1.

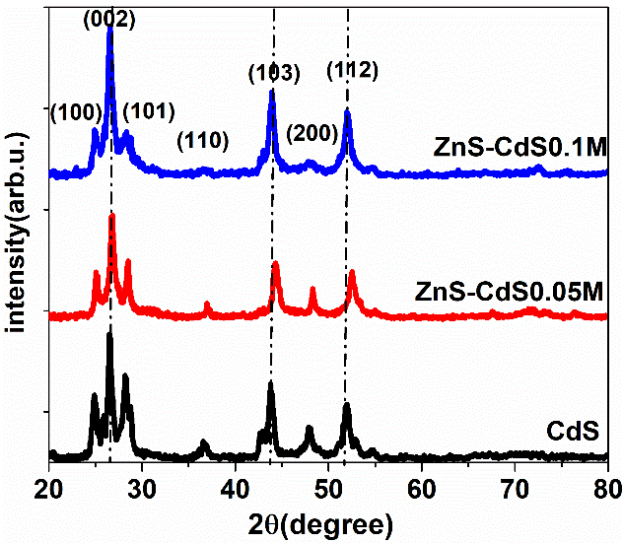

Fig. 1. XRD pattern of preparation nanoparticles.

2.2. UV-Visible spectroscopy

In order to investigate some optical properties of nanoparticles, UV-visible spectroscopy was carried out. These spectra were displayed in Figure 2. The absorption spectrum of the samples (Fig. 2a) shows that the absorption peak position is dependent on Zn content and it will change by adding Zn to the CdS structure. In line with previous studies, the absorbance spectrum of the pure cadmium sulfide was shown at the wavelength of 233 nm.[38]. The absorption peak of the second sample, which was prepared with 0.1 M Zn solution, is 247 nm, and for the third sample, which was prepared with 0.05 M Zn solution, is around 241 nm. This difference in the absorption peaks can indicate the difference in the

bandgap of the synthesized samples.

The band gap of any nanomaterial can be inferred from absorption spectrum using different methods, one of these methods which is widely used by scientists is Tauc method. According to the Tauc equation, the absorption coefficient α is defined as follows[39]:

$$\alpha = \frac{2.303A}{t} \quad (1)$$

Where A and t are absorption and the thickness of the sample, respectively. Then the band gap of semiconductor was calculated using equation 2.

$$ahv = B\left(hv - E_g\right)^n \quad (2)$$

Where hυ is the energy of the photon, B is a constant value and n is the power factor of the transition mode, which is dependent upon the nature of the material, and in materials with direct band gap n is considered to be 0.5. As shown in Figure 2b, the band gap of a semiconductor is equal to the x-intercept of the linear extrapolation of the tangent to the $(\alpha h\nu)^2$ versus hν plot in the appropriate energy region. According to our results, the band gap of cadmium sulfide is about 2.7 eV, which is slightly different from the reported value of 2.4 eV [40, 41]. The gap of the ZnS-CdS samples changed, while the sample with 0.1 molar of Zinc content has a smaller gap in the visible region of about 2.2 eV, and for the sample 0.5M, the measured gap was 2.3 eV. It is clear that by varying the zinc content of these nanocomposites, the band gap changes, therefore by choosing the optimum zinc content, we can reach better conditions for light absorption in the visible region and improvement in the photodegradation of the material under renewable energy sources, so their properties are far better than the pure samples[41, 42].

2.3. SEM and DAX analysis

Scanning Electron Microscopy (SEM) is mainly used to provide useful information on our specimens including their topography, morphology, composition and crystallographic data and Energy-dispersive X-ray analysis (EDAX) is used to determine the percentages of their constituents, therefore our samples have been analyzed with both techniques. The SEM results are shown in Figure 3. All images are at the same scale bar, 200 nm. These images confirm the spherical shape of nanoparticles and this fact has inspired us to simulate the nanocomposites in the same shape. The grain size distribution in our synthesized samples are presented in histogram of SEM images. (Figure 4). The histogram of SEM images (Figure 4) indicates the grain size distribution in our synthesized samples, the dominant grain size in CdS is 60 nm, while it decreases to 50 nm and 40-45 nm in samples of 0.05 and 0.1, respectively. It is clear that samples with smaller size have better photocatalytic activity[43]. So we expect that the sample prepared with 0.1 M zinc is a good photocatalyst.

The results of EDAX analysis, Figure 5, proves that the percentage of zinc in the sample 0.1 M is three times higher than sample 0.05 M.

2.4. Photocatalytic activity

Organic dyes have been used to investigate the photocatalytic activity of prepared nanomaterials. Organic dyes such as RhB were used as pollutants. In the current study, 100 mg of prepared nanopowders was dispersed in 100 ml of 10 ppm RhB solution by ultrasonic bath waves. Then the solution was placed in the dark for half an hour until the system reached the absorption and desorption equilibrium, in the next step the suspension was exposed to SMD light irradiation at 25℃. After 30 minutes, 4 ml of solution was separated from the beaker and after centrifugation and separation of nanopowder, the absorption peak of RhB was measured with Shimadzu's UV-1800 spectrophotometer. Figure 6 shows the

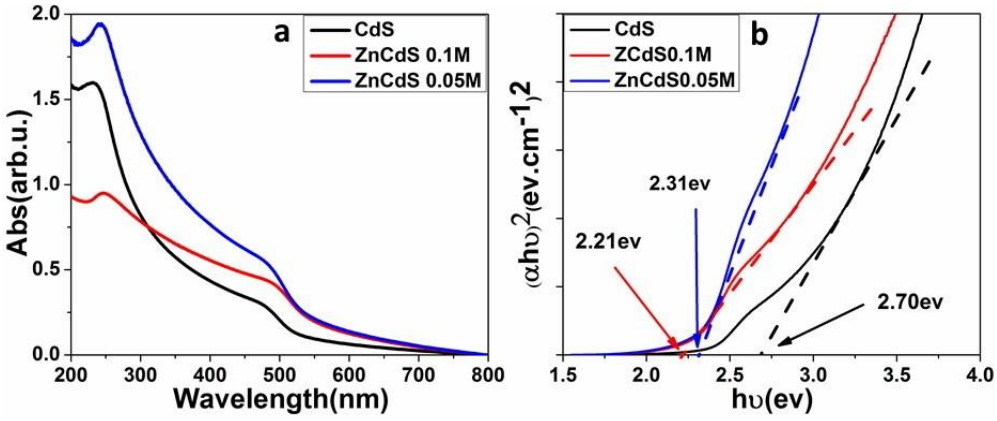

Fig. 2. a) Absorbance spectra and b) Gap calculation of samples.

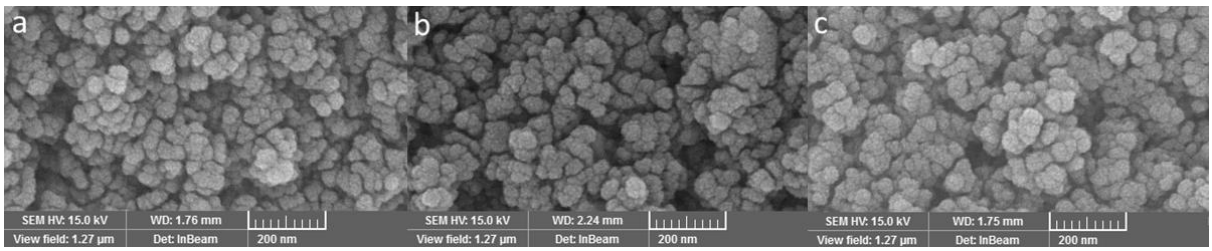

Fig. 3. SEM image of nanocomposites. a) CdS, b) 0.05 M, c) 0.1 M.

percentage of photodegradation of dyes under light. in order to calculate the degradation efficiency of different samples, the following formula was employed [44]:

$$Degradation\ Efficiency\% = \left(\frac{1-A_t}{A_0}\right) \times 100 \qquad (3)$$

Where A_t is the concentration of the pollutant after light irradiation and A_0 is the initial concentration of the pollutant. According to Figure 6a, sample 0.1 M zinc which possess 16% zinc atoms in its structure, has a better photocatalytic activity. i.e. 80% of RhB was degraded after solution exposure to the SMD light for 120 minutes. Considering smaller band gap and smaller size of nanoparticles, these results were anticipated.

For more studies and detailed investigation of the photodegradation of materials and identification of effective nanostructures, the Langmuir-Hinshelwood mechanism is used. The kinetics of the photocatalytic reaction and the rate of degradation are better defined by the Langmuir-Hinshelwood equation, which is expressed as follows[45]:

$$Ln\left(\frac{C}{C_0}\right) = -K_{app}t \qquad (4)$$

C_0 and C are the concentration of the pollutant at the first step and after the degradation, K_{app} and t are the degradation rate and time. Since the natural logarithm of

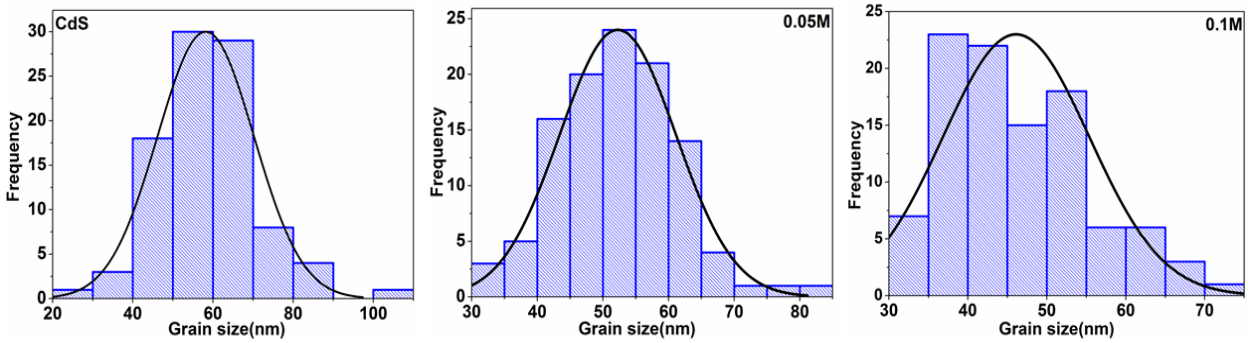

Fig. 4. Histograms corresponding to grain size distributions.

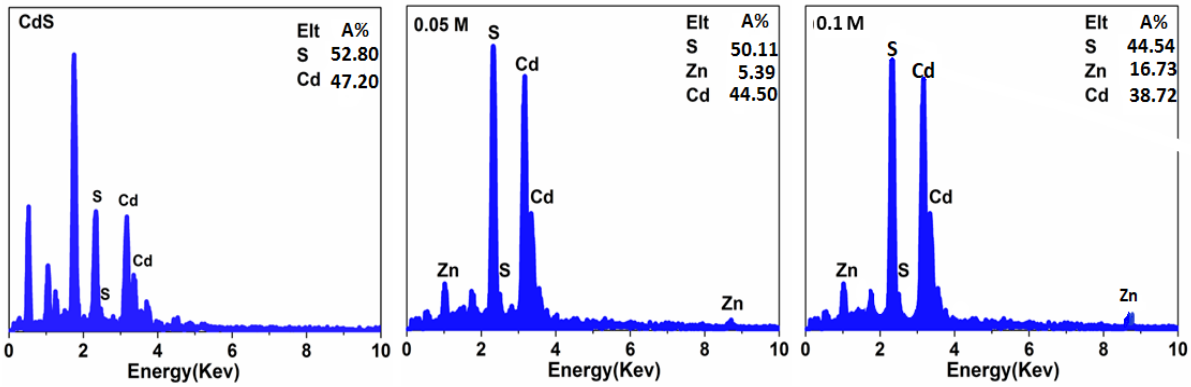

Fig. 5. Energy dispersive X-ray analysis (EDAX) of the synthesized samples.

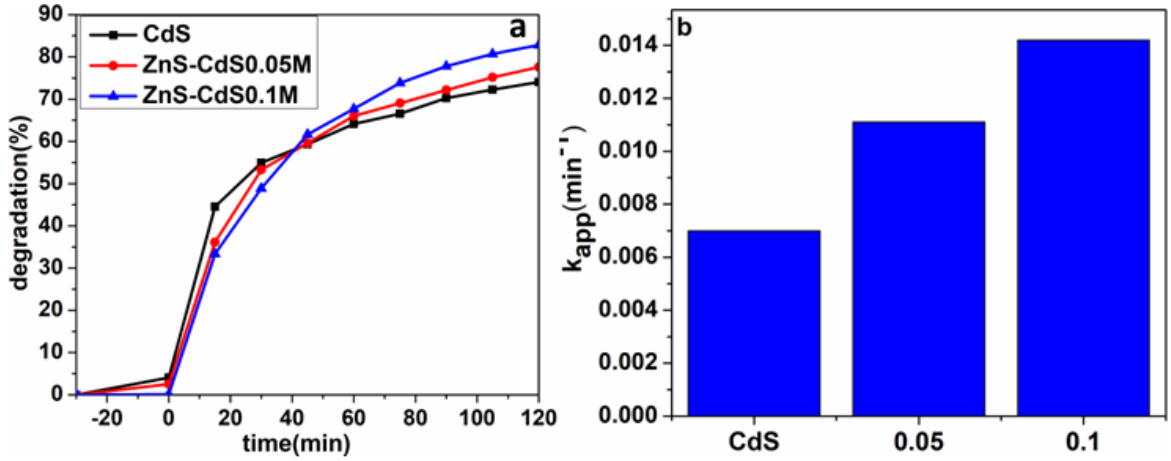

Fig. 6. a) Photodegradation percentage of nanostructures, and b) kinetic of photocatalytic activity by Langmuir-Hinshelwood equation.

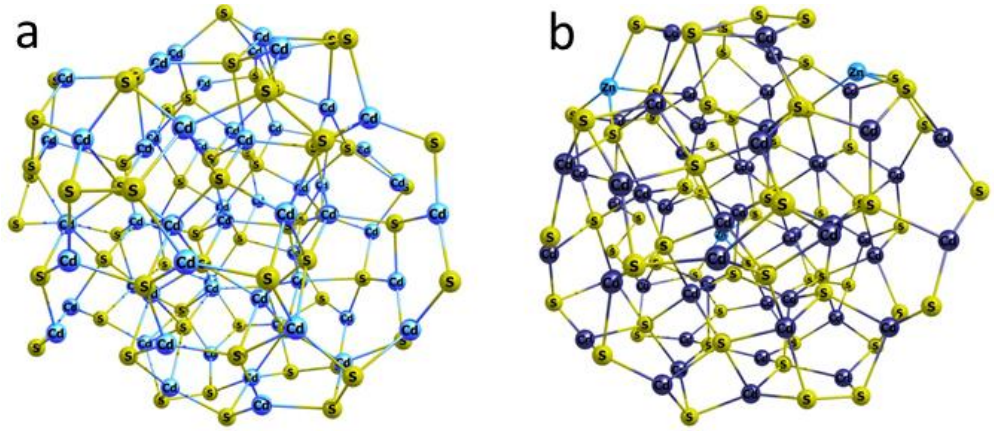

Fig. 7. a) The pure cadmium sulfide structure in the hexagonal phase b) the spherical Zns-CdS structure containing 2.5% of zinc, Zn atoms have been marked by a light blue color.

the concentration of RhB versus time is linear, then the reaction type is first order and its slope yields the degradation rate. The calculated degradation rates of different samples are shown in Figure 6b. Compared to the other samples, the 0.1 M sample exhibits the fastest pollutant removal reaction.

III. Theoretical method

The optical properties and photocatalytic performance of the synthesized materials can also be investigated through theoretical methods. In experimental section, three nanostructures with different Zn content, namely 0%, 5% and 16%, were synthesized, The synthetic process of these specimens are costly and time consuming, while the simulations and the theoretical studies offers a more efficient and cost-effective alternative for exploring their properties, then, we have more flexibility to check the dependence of the band gap of nanostructures on their Zn content. Therefore, these nanomaterials were modeled using ATK and VESTA Softwares in a small molecular cluster scale. Their optical characteristics were analyzed employing various computational methods.

Considering the hexagonal phase and spherical shape of the synthesized nanomaterials which were confirmed in our XRD and SEM studies, we had to keep these characteristics in our computational inputs. The pure cadmium sulfide structure in the hexagonal phase and the spherical ZnS-CdS structure containing 2.5% of zinc are presented in figure 7a and b, respectively. To minimize the computational complexity of simulating larger systems, the molecules were modeled at a reduced size of 20 Å (2 nm).

In molecular systems, electrons are distributed within molecular orbitals, notably the highest occupied molecular orbital (HOMO) and the lowest unoccupied molecular orbital (LUMO). Consequently, the molecular energy gap is formally defined as the energy difference between these two frontier orbitals as follows [46-48]:

$$E_g = E_{LUMO} - E_{HOMO} \quad (5)$$

Correspondingly, in a crystalline solid, electrons occupy discrete energy levels, forming energy bands. The band gap is defined as the energy difference between the valence band (VB), which is primarily filled with electrons, and the conduction band (CB), where electrons can move freely and contribute to electrical conductivity:

$$E_g = E_{VB} - E_{CB} \quad (6)$$

Generally, the band gap is smaller than the HOMO-LUMO gap. When multiple molecules are brought together, intermolecular interactions cause molecular energy levels to shift closer, leading to the formation of broader energy bands. Consequently, in transition from a molecule into a solid, the molecular gap transforms into the band gap, which is usually smaller. The HOMO is analogous to the valence band, while the counterpart of LUMO is the conduction band in solids. In contrast to the band gap, the HOMO-LUMO gap is defined in molecular systems, particularly in finite systems such as single molecules, clusters, and nanostructures. [49].

Moreover, the experimentally measured band gap of our synthesized CdS is larger than the reported values for bulk solids, directly indicating the presence of quantum confinement and surface effects and confirming the nanoscale nature of our synthesized samples [50].

Based on the aforementioned considerations, we are convinced to compare the experimentally measured band gap with the theoretical HOMO-LUMO gap. The input of our simulation is not a single molecule but has a size of approximately 2 nanometers, which can partially justify our approximation.

The positions of the CB and VB edges play a crucial role in hydrogen evolution reactions, as they determine key reaction conditions. For a spontaneous reaction, the CB edge must be equal to or more negative than the proton reduction potential (H_2/H^+). Therefore, selecting an appropriate semiconductor is subject to two conditions: (1) the band gap must fall within the visible range, and (2) the VB position must be more positive than the oxidation potential (H_2O/O_2). These two factors ensure sufficient potential for oxygen production in the water-splitting photocatalytic process[51].

The Hartree-Fock results are summarized in Figure 8. According to HF results the calculated HOMO-LUMO gap is about 7.53 eV which has significant difference with

our experimental results, i.e. 2.7 eV. Therefore, the Hartree-Fock method was replaced with more advanced methods including B3lyp, M05 and M06 in our calculations.

This functional was employed to determine the band gap of the modeled nanostructures. The M05 results are shown in figure 9(a). Fairly good consistency is seen between our experimental gap for pure CdS, calculated gap and its reported gap, 2.7, 2.47 and 2.4 eV,

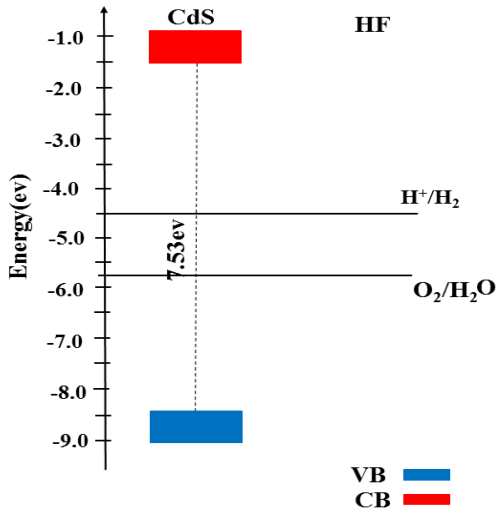

Fig. 8. The calculation of gaps and CB and VB for CdS using the HF method.

respectively. According to M05 results, by embodying zinc into pure CdS structure, the band gap will decrease. This result was confirmed with our experimental findings. For the sample containing 10% zinc, the band gap decreased to 1.8 eV. However, in the sample with 15% zinc, the band gap has slightly increased to 2.03 eV.

Figure 9(b) presents the band gap calculations obtained using the M06 method. The calculated band gap of CdS has clear differnces with experimental values but the trends of variation of the band gap with Zn content is still valid in M06 method. As shown in Figure 9 (b), the minimum band gap occurs on 15% Zn content. by insertion of ZnS in CdS structure up to 2.5%, the band gap increases and it remains almost constant for the structures with 5% and 10% of Zn content, and and in the structure with 15% zinc concentration it decreases, and again it rises with further zinc incorporation. Both computational M05 and M06 results, are inline with experimental findings, which proposes that the nanostructure containing 15% of ZnS will have the mimimal energy gap, therefore a higher photocatalytic performance is anticipated.

The most common hybrid functional, B3LYP was exploited in the current study. As shown in figure 10, the calculated energy gaps are in agreement with the experimental value (1.7 eV). With the addition of zinc to the structure, the band gap suddenly decreases about 11%, and then it remains almost constant for structures containing 2.5,5,10 and 15% of Zn. In structures with 20 and 22.5% of Zn content, this gap will increase to 1.6 eV. Based on Figure 10, the samples with 10 % and 15 % zinc are particularly suitable for the photocatalytic applications due to their smaller band gaps and the favorable band positions. These results further support the experimental findings discussed in the previous section.

The results of the two other computational methods, M06-L and M06-2X, are shown in Figure 11. None of these methods provided an exact match for the band gap value. The M06-2X calculated the band gap to be approximately 3.29 eV, while the M06-L yielded a value of about 1.39 eV for CdS. As seen in Figure 11(a), the M06-2X method does not align with our expectations for band gap calculations. Unlike the previous methods, in M06-2X calculations, the band gap increases with the incorporation of zinc. Specifically, for samples containing 10% and 15% of zinc, the calculated band gaps were approximately 4.47 eV and 3.45 eV, respectively which are far beyond our expectations, Figure 11(a). In the M06-L method, the band gap does not obey a single trend and it simply fluctuates, Figure 11(b). Despite these methods give a quite unrealistic results, but based on the position of band edges and reduction and oxidation potentials, M06-L proposes that the structure with 10% zinc has a better photocatalytic activity. The discrepancy between experimental and theoretical values can be attributed to various factors, including imperfections in experimental results.

In practice, experiments may encounter challenges such as manufacturing defects, misalignment, measurement errors, uncertainties in instrumentation, and systematic errors, all of these factors can contribute to the differences observed between experimental and theoretical outcomes[52].

IV. Future Directions

Application of the following listed ideas is proposed for future studies.

Preparation of diverse nanocomposites based on

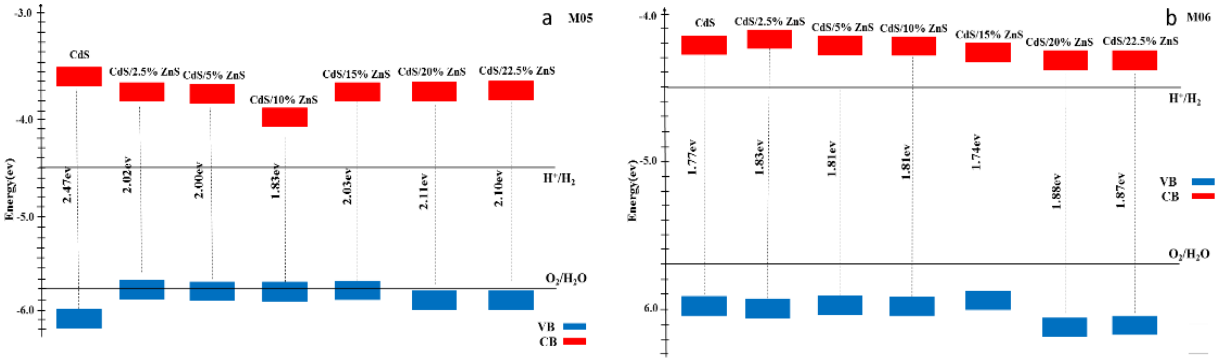

Fig .9. The Band gap of ZnS-CdS nanocomposites calculated by a) M05 and b) M06 functionals.

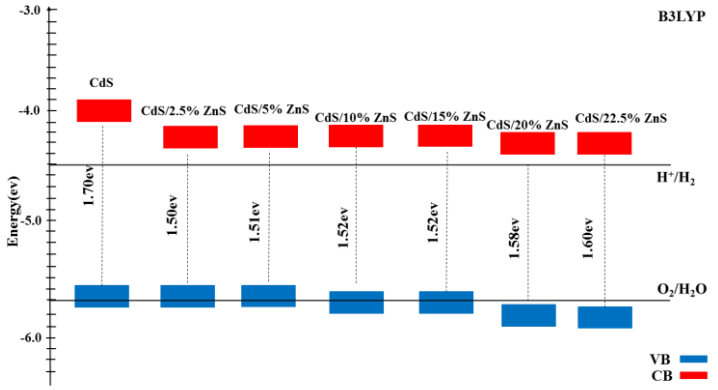

Fig. 10. The Band gap of ZnS-CdS nanocomposites calculated by B3LYP functional.

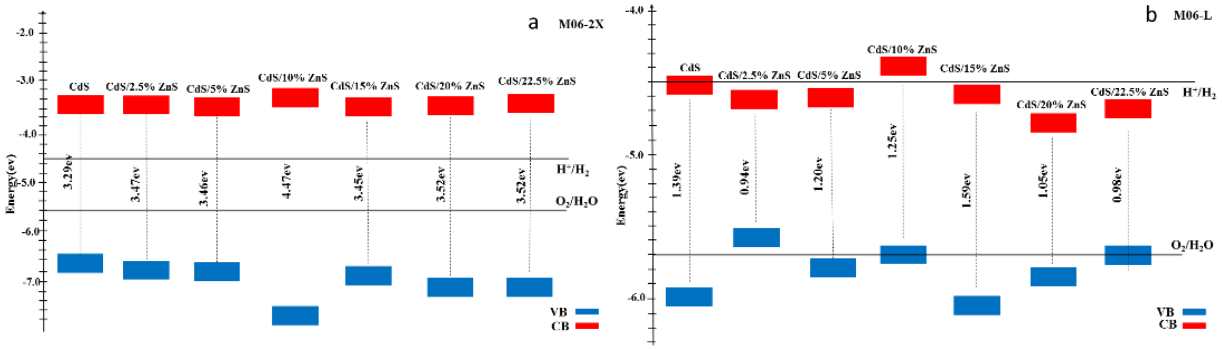

Fig. 11. The Band gap of ZnS-CdS nanocomposites calculated by a) M06-2X and b) M06-2L functional.

cadmium sulfide such as Ag_2S-CdS, MnS-CdS and etc

Experimentally and theoretically investigation of Ag_2S-CdS and MnS-CdS optical properties.

Molecular simulations at larger sizes and the use of more advanced and accurate computational methods.

Simulation of various nanocomposites with different doping percentages of graphene.

Conclusion

In this study, CdS-ZnS nanocomposites with varying zinc content were synthesized using the hydrothermal method. The crystallite size, grain size, surface morphology, and band gap were characterized using XRD, FE-SEM, and UV-VIS techniques. The results demonstrated that the CdS-ZnS nanocomposites were synthesized in the hexagonal phase at the nanoscale. By increasing the zinc content, the calculated band gaps as well as nano crystal size have decreased. These energy gaps are in the visible region.

Experimental photocatalytic tests demonstrated that the CdS-16%ZnS nanocomposite efficiently degraded Rhodamine B (RhB) under SMD irradiation. Theoretical calculations, showed that the M05 functional has good agreement with the experimental results, while it proposes that CdS-10%ZnS sample is a promising photocatalytic candidate.

Funding

This work is supported by Sahand University of Technology with contract number 23681.

Consent to participate

The authors declare their consent for publication.

Declaration of competing interest

The authors promulgate that they have no known competing financial profits or personal relationships that could have appeared to affect the results reported in this manuscript.

Fakhri-Mirzanagh S. – Ph.D Candidate, Faculty of Science, Sahand University of Technology, Tabriz, Iran;
Shojaei S. H. R. – Associate Professor, Faculty of Science, Sahand University of Technology, Tabriz, Iran;
Pirgholi-Givi G. R. –Assistant Professor, Department of Advanced Technologies, University of Mohaghegh Ardabili, Namin, Iran;
Azizian-Kalandara Y.– Department of Physics, University of Mohaghegh Ardabili, P.O. Box.179, Ardabil, Iran. Photonics Department, Applied Science Faculty, Gazi University, Ankara, Turkey

[1] C.E. de Moura, et al., *Experimental and theoretical study of resonant core-hole spectroscopies of gas-phase free-base phthalocyanine*. Physical Chemistry Chemical Physics, 25(22), 15555 (2023); https://doi.org/10.1039/D3CP01746J.

[2] I.R. Ariyarathna, *Wavefunction theory and density functional theory analysis of ground and excited electronic states of TaB and WB*. Physical Chemistry Chemical Physics, 26(35), 22858 (2024); https://doi.org/10.1039/D4CP02202E.
[3] V. Sokolovskiy, et al., *Meta-GGA SCAN functional in the prediction of ground state properties of magnetic materials: Review of the current state.* Metals, 13(4), 728 (2023); https://doi.org/10.3390/met13040728.
[4] W. Kohn, A.D. Becke, and R.G. Parr, *Density functional theory of electronic structure.* The journal of physical chemistry, 100(31), 12974 (1996); https://doi.org/10.1021/jp960669l.
[5] G.E. Scuseria, and V.N. Staroverov, *Progress in the development of exchange-correlation functionals, in Theory and applications of computational chemistry*. Elsevier. 669-724. (2005).
[6] P. Mori-Sánchez, A.J. Cohen, and W. Yang, *Many-electron self-interaction error in approximate density functionals*. The Journal of chemical physics, 125(20), 201102 (2006); https://doi.org/10.1063/1.2403848.
[7] T. Sato, T. Tsuneda, and K. Hirao, *Long-range corrected density functional study on weakly bound systems: Balanced descriptions of various types of molecular interactions.* The Journal of chemical physics, 126(23), 234114 (2007); https://doi.org/10.1063/1.2747243.
[8] Y. Zhao, and D.G. Truhlar, *Density functionals with broad applicability in chemistry.* Accounts of chemical research, 41(2), 157 (2008); https://doi.org/10.1021/ar700111a.
[9] J.M. Crowley, J. Tahir-Kheli, and W.A. Goddard III, *Resolution of the band gap prediction problem for materials design.* The journal of physical chemistry letters, 7(7), 1198 (2016); https://doi.org/10.1021/acs.jpclett.5b02870.
[10] L. Qiao, et al., *Nature of the band gap and origin of the electro-/photo-activity of Co 3 O 4.* Journal of Materials Chemistry C, 1(31), 4628 (2013); https://doi.org/10.1039/C3TC30861H.
[11] K. Takarabe, et al., *Electronic structure of C2N2X (X= O, NH, CH2): Wide band gap semiconductors.* Journal of Applied Physics, 112(1), 013537 (2012); https://doi.org/10.1063/1.4731749.
[12] M. Schlüter, and L. Sham, *Density-functional theory of the band gap, in Advances in quantum chemistry.* Elsevier. 21, 97 (1990); https://doi.org/10.1016/S0065-3276(08)60593-6.
[13] J.K. Perry, J. Tahir-Kheli, and W.A. Goddard III, *Antiferromagnetic band structure of la 2 cuo 4: Becke-3–lee-yang-parr calculations*. Physical Review B, 63(14), 144510 (2001); https://doi.org/10.1103/PhysRevB.63.144510.
[14] A. Seidl, et al., *Generalized Kohn-Sham schemes and the band-gap problem.* Physical Review B, 53(7), 3764 (1996); https://doi.org/10.1103/PhysRevB.53.3764.
[15] J. Muscat, A. Wander, and N. Harrison, *On the prediction of band gaps from hybrid functional theory.* Chemical Physics Letters, 342(3-4), 397 (2001); https://doi.org/10.1016/S0009-2614(01)00616-9.
[16] J. Heyd, et al., *Energy band gaps and lattice parameters evaluated with the Heyd-Scuseria-Ernzerhof screened hybrid functional.* The Journal of chemical physics, 123(17), 174101 (2005); https://doi.org/10.1063/1.2085170.
[17] A.J. Cohen, P. Mori-Sánchez, and W. Yang, *Fractional charge perspective on the band gap in density-functional theory*. Physical Review B—Condensed Matter and Materials Physics, 77(11); 115123 (2008); https://doi.org/10.1103/PhysRevB.77.115123.
[18] A.J. Garza, and G.E. Scuseria, *Predicting band gaps with hybrid density functional*s. The journal of physical chemistry letters, 7(20), 4165 (2016); https://doi.org/10.1021/acs.jpclett.6b01807.
[19] J.P. Perdew, et al., *Understanding band gaps of solids in generalized Kohn–Sham theory.* Proceedings of the national academy of sciences, 114(11), 2801 (2017); https://doi.org/10.1073/pnas.1621352114.
[20] M.K. Chan, and G. Ceder, *Efficient band gap prediction for solids.* Physical review letters, 105(19), 196403 (2010); https://doi.org/10.1103/PhysRevLett.105.196403.
[21] J. Heyd, G.E. Scuseria, and M. Ernzerhof, *Hybrid functionals based on a screened Coulomb potential.* The Journal of chemical physics, 118(18), 8207 (2003); https://doi.org/10.1063/1.1564060.
[22] J.E. Moussa, P.A. Schultz, and J.R. Chelikowsky, *Analysis of the Heyd-Scuseria-Ernzerhof density functional parameter space.* The Journal of chemical physics, 136(20), 204117 (2012); https://doi.org/10.1063/1.4722993.
[23] H. Xiao, J. Tahir-Kheli, and W.A. Goddard III, *Accurate band gaps for semiconductors from density functional theory*. The Journal of Physical Chemistry Letters, 2(3), 212 (2011); https://doi.org/10.1021/jz101565j.
[24] S.U. Hong, et al., *Density functional theory calculations for the band gap and formation energy of* $Pr_{4-x}Ca_xSi_{12}O_{3+x}N_{18-x}$ *a highly disordered compound with low symmetry and a large cell size.* Physical Chemistry Chemical Physics, 19(25) 16702 (2017); https://doi.org/10.1039/C7CP03247A.
[25] B.J. Abdullah, *Size effect of band gap in semiconductor nanocrystals and nanostructures from density functional theory within HSE06.* Materials Science in Semiconductor Processing, 137, 106214 (2022); https://doi.org/10.1016/j.mssp.2021.106214.
[26] A. Kumar, and G. Pandey, *A review on the factors affecting the photocatalytic degradation of hazardous materials*. Mater. Sci. Eng. Int. J, 1(3), 106 (2017); 10.15406/mseij.2017.01.00018.
[27] F.T. Geldasa, et al., *Experimental and computational study of metal oxide nanoparticles for the photocatalytic degradation of organic pollutants: a review.* RSC advances, 13(27), 18404 (2023); https://doi.org/10.1039/D3RA01505J.
[28] L. Lianmawii, et al., *A review: photocatalytic degradation of dyes by metal sulfide nanoparticle*s. Brazilian Journal of Chemical Engineering, 1 (2024); https://doi.org/10.1007/s43153-023-00425-9.
[29] N. Kozhevnikova, et al., *Janus ZnS nanoparticles: Synthesis and photocatalytic properties*. Journal of Physics and Chemistry of Solids, 161, 110459 (2022); https://doi.org/10.1016/j.jpcs.2021.110459.

[30] H. Abdulelah, et al., *Photocatalytic Activity to Remove the Effect of Methylene Blue Dye by Using CdS Nanocrystalline under Visible Light.* Journal of Nanostructures, 14(2), 370 (2024); https://doi.org/10.22052/JNS.2024.02.002.

[31] A. Hernández-Gordillo, F. Tzompantzi, and R. Gómez, *An efficient ZnS-UV photocatalysts generated in situ from ZnS (en) 0.5 hybrid during the H2 production in methanol–water solution*. International journal of hydrogen energy, 37(22), 17002 (2012); https://doi.org/10.1016/j.ijhydene.2012.08.097.

[32] Z.K. Heiba, et al., *Influence of (Mn or Co)-doping on structural, magnetic and electronic properties of nano Zn0. 75Cd0. 25S*. Chinese Journal of Physics, 67, 414 (2020); https://doi.org/10.1016/j.cjph.2020.04.010.

[33] M. Khodamorady, and K. Bahrami, *A novel ZnS-CdS nanocomposite as a visible active photocatalyst for degradation of synthetic and real wastewaters*. Scientific Reports, 13(1), 2177 (2023); https://doi.org/10.1038/s41598-023-28725-7.

[34] I. Devadoss, P. Sakthivel, and A. Krishnamoorthy, B*and gap tailoring and photoluminescence performance of Cds quantum dots for white LED applications: Influence of Ba 2+ and Zn 2+ ions.* Journal of Materials Science: Materials in Electronics, 32, 5729 (2021); https://doi.org/10.1007/s10854-021-05293-y.

[35] P. Baláž, et al., *CdS/ZnS nanocomposites: from mechanochemical synthesis to cytotoxicity issues.* Materials Science and Engineering: C, 58, 1016 (2016); https://doi.org/10.1016/j.msec.2015.09.040.

[36] I. Vamvasakis, E.K. Andreou, and G.S. Armatas, *Mesoporous Dual-Semiconductor ZnS/CdS Nanocomposites as Efficient Visible Light Photocatalysts for Hydrogen Generation*. Nanomaterials, 13(17), 2426 (2023); https://doi.org/10.3390/nano13172426.

[37] N. Prasad, and B. Karthikeyan, *Phase-dependent structural, optical, phonon and UV sensing properties of ZnS nanoparticles*. Nanotechnology, 30(48), 485702 (2019); https://doi.org/10.1088/1361-6528/ab3cbf.

[38] R. Tripathi, et al., *Mechanistic aspects of biogenic synthesis of CdS nanoparticles using Bacillus licheniformis*. Advances in Natural Sciences: Nanoscience and Nanotechnology, 5(2), 025006 (2014); https://doi.org/10.1088/2043-6262/5/2/025006.

[39] J. Kiwi, and V. Nadtochenko, *New evidence for TiO2 photocatalysis during bilayer lipid peroxidation.* The Journal of Physical Chemistry B, 108(45), 17675 (2004); https://doi.org/10.1021/jp048281a.

[40] G. Martínez-Castañón, *Synthesis of CdS nanoparticles: a simple method in aqueous media.* Advances in Technology of Materials and Materials Processing Journal(ATM), 7(2), 171 (2005).

[41] N. Soltani, et al., *Visible light-induced degradation of methylene blue in the presence of photocatalytic ZnS and CdS nanoparticles*. International journal of molecular sciences, 13(10), 12242 (2012); https://doi.org/10.3390/ijms131012242.

[42] D. Sudha, and P. Sivakumar, *Review on the photocatalytic activity of various composite catalysts.* Chemical Engineering and Processing: Process Intensification, 97, 112 (2015). https://doi.org/10.1016/j.cep.2015.08.006.

[43] D. Li, et al., *Effects of particle size on the structure and photocatalytic performance by alkali-treated TiO2*. Nanomaterials, 10(3), 546 (2020); https://doi.org/10.3390/nano10030546.

[44] S. Fakhri-Mirzanagh, et al., *The effect of graphene oxide content on the photocatalytic activity of (ZnCdS/MnFe2O4/GO) nanocomposite.* Physica B: Condensed Matter, 685, 415974 (2024); https://doi.org/10.1016/j.physb.2024.415974.

[45] I. Matsuura, M. ImaizumI, and M. Sugiyama, *Method of kinetic analysis of photodegradation: nifedipine in solutions.* Chemical and pharmaceutical bulletin, 38(6), 1692 (1990); https://doi.org/10.1248/cpb.38.1692.

[46] M.L. Jabbar, and K.J. Kadhim, *Electronic properties of doped graphene nanoribbon and the electron distribution contours: A DFT study*. Russian Journal of Physical Chemistry B, 15, 46 (2021); https://doi.org/10.1134/S1990793121010188.

[47] H Muzel, M., A.S. Alwan, and M.L. Jabbar, *Electronical Properties for (CxHyZ2-NO) Nanoclusters*. Current Nanomaterials, 2(1), 33 (2017); https://doi.org/10.2174/2405461502666170227121949.

[48] M.L. Jabbar, and K.J. Kadhim. Linear & nonlinear optical properties of undoped & doped graphene nanoribbon via TD-DFT study. in AIP Conference Proceedings. 2020. AIP Publishing.

[49] C. Kittel, and P. McEuen, *Introduction to solid state physics.* 2018: John Wiley & Sons.

[50] D. Bharti, A.V. Bharati, and A.V. Wankhade, *Synthesis, characterization and optical property investigation of CdS nanoparticles*. Luminescence, 33(8), 1445 (2018); https://doi.org/10.1002/bio.3572

[51] N. Goodarzi, et al., *Recent progress on semiconductor heterogeneous photocatalysts in clean energy production and environmental remediation.* Catalysts, 13(7), 1102 (2023); https://doi.org/10.3390/catal13071102.

[52] K.J. Kuipers, and S.J. Hysom, *Common problems and solutions in experiments, in Laboratory experiments in the social sciences*. Elsevier. 145 (2014).

С. Фахрі-Мірзанагх[1], С.Х.Р. Шоджаї[1,2], Г. Р. Пірголі-Гіві[3], Ю. Азізян-Каландараг[4,5,6]

Теоретичні та експериментальні дослідження ширини забороненої зони бінарних нанокомпозитів ZnS-CdS як найкращих очікуваних фотокаталізаторів

[1]Кафедра фізики, факультет природничих наук, Технологічний університет Саханда, Тебріз, Іран;
[2]X-LAB, Університет Хассельта, Агоралаан, Діпенбек, Бельгія, shojaei@sut.ac.ir;
[3]Кафедра передових технологій, Університет Мохагхег Ардабілі, Намін, Ісламська Республіка Іран;
[4]Центр застосування та досліджень фотоніки, Університет Газі, Анкара, Туреччина;
[5]Кафедра фотоніки, факультет прикладних наук, Університет Газі, Анкара, Туреччина;
[6]Кафедра фізики, Університет Мохаге Ардабілі, Ардебіль, Іран

Нанокомпозити ZnS-CdS синтезовано гідротермічним методом для дослідження їхньої фотокаталітичної активності. Результати рентгенівської дифракції (XRD) підтвердили формування гексагональної структури нанокомпозитів сульфіду кадмію та сульфіду цинку, а результати скануючої електронної спектроскопії (SEM) показали, що при додаванні ZnS до структури сульфіду кадмію розмір наночастинок зменшується, що є чіткою ознакою покращеної фотокаталітичної активності. Використовуючи коефіцієнт поглинання та УФ-видиму спектроскопію (УФ), визначено ширину забороненої зони чистого CdS на рівні 2,7 еВ; при додаванні вмісту Zn ширина забороненої зони зменшується. Фотокаталітичну активність отриманих нанокомпозитів вивчали шляхом фотодеградації органічного барвника родаміну B (RhB). Синтезований зразок з 0,1 M розчином цинку показав менші ширину та розмір. На наступному етапі було змодельовано наночастинки сульфіду кадмію з різним відсотковим вмістом цинку, а їхні ширини HOMO-LUMO розраховано за допомогою теорії функціоналу густини (DFT). Порівняно з іншими відомими функціоналами, виявлено, що M05 демонструє кращу відповідність з експериментальними результатами. Результати обчислень підтверджують, що зразок з 10% вмістом цинку є хорошим кандидатом для фотокаталітичної активності.

Ключові слова: Гідротермальний метод, фотокаталітична активність, родамін B, енергетчна щілина, теорія функціоналу густини.